Biogeosciences Discuss., 6, 9849–9889, 2009
www.biogeosciences-discuss.net/6/9849/2009/

Biogeosciences Discussions

Biogeosciences Discussions is the access reviewed discussion forum of *Biogeosciences*

Atmospheric deposition of nutrients and excess N formation in the North Atlantic

L. M. Zamora[1], **A. Landolfi**[2], **A. Oschlies**[2], **D. Hansell**[1], **H. Dietze**[2], **and F. Dentener**[3]

[1]Rosenstiel School of Marine and Atmospheric Science, University of Miami, Miami, USA
[2]IFM-GEOMAR, Leibniz-Institut für Meereswissenschaften an der Universität Kiel, Kiel, Germany
[3]European Commission, Institute for Environment and Sustainability, Joint Research Centre, Ispra, Italy

Received: 16 September 2009 – Accepted: 21 September 2009 – Published: 14 October 2009

Correspondence to: L. Zamora (lzamora@rsmas.miami.edu)

Published by Copernicus Publications on behalf of the European Geosciences Union.

Abstract

Anthropogenic emissions of nitrogen (N) to the atmosphere have been strongly increasing during the last century, leading to greater atmospheric N deposition to the oceans. The North Atlantic subtropical gyre (NASTG) is particularly impacted. Here, upwind sources of anthropogenic N from North American and European sources have raised atmospheric N deposition to rates comparable with N_2 fixation in the gyre. However, the biogeochemical fate of the deposited N is unclear because there is no detectable accumulation in the surface waters. Most likely, deposited N accumulates in the main thermocline instead, where there is a globally unique pool of N in excess of the canonical Redfield ratio of 16 N:1 phosphorus (P). To investigate this depth zone as a sink for atmospheric N, we used a biogeochemical ocean transport model and year 2000 nutrient deposition data. We examined the maximum effects of three mechanisms that may transport excess N from the ocean surface to the main thermocline: physical transport, preferential P remineralization of sinking particles, and nutrient uptake and export by phytoplankton at higher than Redfield N:P ratios. Our results indicate that atmospheric deposition may contribute 13–19% of the annual excess N input to the main thermocline. Modeled nutrient distributions in the NASTG were comparable to observations only when non-Redfield dynamics were invoked. Preferential P remineralization could not produce realistic results on its own; if it is an important contributor to ocean biogeochemistry, it must co-occur with N_2 fixation. The results suggest that: 1) the main thermocline is an important sink for anthropogenic N deposition, 2) non-Redfield surface dynamics determine the biogeochemical fate of atmospherically deposited nutrients, and 3) atmospheric N accumulation in the main thermocline has long term impacts on surface ocean biology.

BGD

6, 9849–9889, 2009

1 Introduction

Atmospheric deposition of N to the ocean has greatly increased over the past 200 years with the intensification of anthropogenic N production from agricultural and fossil fuel sources (Duce et al., 2008; Galloway, 2008). The North Atlantic subtropical gyre (NASTG) is particularly affected by increased deposition because it is very nutrient impoverished and it is located downwind of highly industrialized continents. As atmospheric N deposition to the NASTG has more than doubled since 1860 (Galloway, 1996), the process has become an increasingly important new source of N to marine organisms there (Krishnamurthy et al., 2007).

The fate of atmospheric N deposited in the NASTG is unclear because the nutrient dynamics are incompletely understood. Phosphate concentrations at the surface are very low (often <1 nM) (Wu et al., 2000; Li and Hansell, 2008), and because deposition has high N:P ratios, typically ranging from 100:1 to 300:1 (e.g. Markaki et al., 2003; Chen et al., 2007), one might expect deposited N to accumulate in the surface waters before being transported from the surface into the main thermocline via subduction (or sinking). Although we cannot exclude changes on longer timescales, increases in the concentrations of N have not been observed in the gyre surface in the past 20 years (Fig. 1). This lack in increase in surface N indicates that the estimated 0.1 mol N m^{-2} yr^{-1} (obtained from Dentener et al., 2006) deposited to the surface is removed at a rate approximating its input.

Export to the main thermocline is one apparent fate for excess N deposited to the subtropical North Atlantic. In the depth range of 200–800 m (Fig. 2), high inorganic N:P ratios relative to Redfield values (16 N:1P on a molar basis) (Redfield et al., 1963) have long been noted (Fanning, 1992). The indices N*, DINxs and TNxs have been used to describe the N in excess of the canonical Redfield ratio (Gruber, 1997; Hansell et al., 2004; Landolfi et al., 2008). TNxs, which includes organic nitrogen and phosphorus, would be the ideal index to use to describe basin-wide biogeochemistry because organic matter is an important pool of nutrients at the surface (Fig. 1; Bronk, 2002;

BGD
6, 9849–9889, 2009

Karl and Björkman, 2002). However, because there are not enough dissolved organic nitrogen (DON) and phosphorus (DOP) data to meaningfully map distributions in the NASTG, and because the organic DON and DOP fractions in deposition are not well understood, here we restrict ourselves to the use of inorganic N (DIN) and P (DIP). We employ the index DINxs, which is defined as the excess of inorganic N relative to inorganic P expected from the Redfield relationship:

$$\mathrm{DINxs} = [\mathrm{NO_3^-}] - 16 * [\mathrm{PO_4^{3+}}] \quad (1)$$

Along with the input of high N:P atmospheric material, other suggested sources of elevated DINxs levels in the NASTG include mineralization of high N:P diazotrophic particles and subduction of high N:P dissolved organic matter (DOM) (Fanning, 1992; Gruber, 1997; Pahlow and Riebesell, 2000; Deutsch et al., 2007; Hansell et al., 2007). The relative contributions of atmospheric N deposition and N_2 fixation are particularly difficult to determine (Hansell et al., 2007) because both inputs have similar biogeochemical signatures (i.e., light isotopic N signatures (Knapp, 2009) and high N:P ratios). Another unknown is the mechanisms for excess N from N_2 fixation and atmospheric deposition to reach the depths of the main thermocline from the surface layer.

Both the biological response and the physical transport of water are key to the eventual fate of the deposited nutrients. Thus, in the present study we examine three of the most likely transport mechanisms: transport by advection and subduction, preferential P remineralization in sinking particles, and non-Redfield nutrient uptake and export in phytoplankton (Fig. 3). The first mechanism is simple physical transport of deposited excess N, assessed here in what we call the "Redfield scenario". If all biological processes occur in Redfield ratios, then deposited excess N should be retained in the surface layer until it is either transported out of the system by advection or to depth through physical processes like subduction. Any deposited N not taken up by and retained in the biological system (i.e., as biomass at Redfield ratio) would then act similarly to a passive tracer, perhaps being present as DON in the real ocean, following uptake and release by the autotrophs.

The second mechanism for transport of excess N to depth occurs when P is preferentially remineralized in the surface with respect to N (referred to here as the "preferential P remineralization scenario"). If P is more readily mineralized from sinking biogenic particles than N, a particle initially at Redfield N:P ratios will become N-enriched as it sinks. In this scenario, phosphorus would be more efficiently recycled and retained in surface waters, lessening P depletion and enabling continued production with further N deposition. At the same time, sinking N-enriched particles would keep surface water N levels low, and upon mineralization in the main thermocline would form the enriched DINxs signal found there. Evidence of differential remineralization rates comes from vertical gradients in the molar ratios of DON and DOP (Vidal et al., 1999; Abell et al., 2000; Aminot et al., 2004; Landolfi et al., 2008). N:P enrichment of particles at depth may also be partially explained by preferential P remineralization (Anita, 2005).

The third mechanism for the transport of atmospheric excess N to the main thermocline is through the growth and sinking of particles that are formed at higher than Redfield ratios (referred to here as the "excess N uptake scenario"). This process is hypothesized to be caused by changes in the optimal biochemical makeup of phytoplankton under nutrient stress (Arrigo, 2005; Pahlow and Oschlies, 2009), and has been observed in some phytoplankton in the NASTG (e.g. Lomas et al., 2004; Van Mooy et al., 2009). The high N:P ratios of particles found in sediment traps could also be explained, at least in part, by this process.

The three scenarios are expected to result in markedly different vertical gradients when implemented in a model, both at the surface and in the main thermocline. We used a 3-D global biogeochemical-ocean transport model to isolate the simulated effects of these three mechanisms. By observing the biogeochemical signatures of the three mechanisms in the water column, we are able to 1) identify which mechanisms best simulate the observed nutrient patterns, 2) compare the production rates of DINxs and ADINxs (where ADINxs is the fraction of the DINxs pool in the main thermocline coming from atmospheric deposition), and 3) approximate the importance of atmospheric deposition to total excess N formation in the main thermocline of the subtropical

BGD
6, 9849–9889, 2009

North Atlantic. Overall, we seek to better assess the functioning of the North Atlantic subtropical gyre nutrient system and how it may respond in the future to increased N inputs from the atmosphere.

2 Methods

2.1 Atmospheric nutrient deposition to the ocean

Year 2000-level deposition of wet and dry inorganic nitrogen was obtained at a one degree resolution from the mean of 23 atmospheric chemistry transport models (Dentener et al., 2006). Compared to measurements, the mean model showed relatively good performance over the North American and European source regions; also comparison over the few available coastal and open ocean measurements was relatively good (Dentener et al., 2006). Inorganic nitrogen deposition (Fig. 4a) applied to the biogeochemical ocean model included NO_y (NO, NO_2, HNO_3, HNO_4, NO_3, $2\times N_2O_5$, PAN, organic nitrates) and NH_x (NH_3 and NH_4).

Observations of soluble reactive phosphorus (SRP) deposition are sparse; because there are more data for comparison, we focused on comparison with total phosphorus (TP) deposition in our study instead. Since the two main sources of total phosphorus in deposition are dust and combustion processes (Mahowald et al., 2008), we estimated TP deposition (Fig. 4b) from maps of dust and black carbon (BC) (BC is a proxy for combustion sources). TP was estimated from BC deposition by assuming TP is equally divided between coarse and fine fractions and by using published BC:TP molar ratios of 0.02 (for coarse particles) and 0.0029 (for fine particles) (Mahowald et al., 2005). P derived from dust was estimated from a dust:TP ratio of 7×10^{-4} (Taylor and McLennan, 1995). BC and dust deposition maps were averaged from five atmospheric chemistry models made available by the AeroCom project (the GISS, LOA, LSCE, MATCH, and PNNL models).

The contribution of organic N in deposition was not included in the model. Solu-

BGD
6, 9849–9889, 2009

ble organic nitrogen in deposition is likely to be at least partially bioavailable (Peierls and Paerl, 1997; Seitzinger and Sanders, 1999; Duarte et al., 2006) and has been estimated to be 30% of the inorganic N values (Duce et al., 2008), although sources to the subtropical North Atlantic may be less than that (Zamora et al., 2009). The sources, distributions, bioavailability and lifetime of these compounds, however, are not well known. Therefore, organic N compounds other than organic nitrates were excluded. Even less is known about soluble organic P in deposition, but the existing literature indicates that organic P does not outweigh the large excess of N with respect to Redfield ratios (e.g. Graham et al., 1979; Chen et al., 2007).

2.2 Circulation model

Global ocean circulation was simulated by the Modular Ocean Model Version 4p0d (MOM4) from the Geophysical Fluid Dynamics Laboratory (GFDL) in Princeton, New Jersey. The MOM4 model was driven by climatological forcing following the Coordinated Ocean Reference Experiments (CORE) (based on Large and Yeager, 2004). Model configuration corresponds to that used in GFDL's coupled climate model CM2.1 (Griffies et al., 2005; Gnanadesikan, 2006). The model was initialized with annual mean temperature and salinity from the World Ocean Atlas 2001 (Boyer et al., 2002; Stephens et al., 2002) and was run with a $2^{\circ} \times 3^{\circ}$ horizontal resolution and 28 vertical layers. Atmospheric N and P, interpolated from the monthly deposition maps described above, were added to the uppermost grid box. For conceptual simplicity, we used year 2000 deposition estimates for each year of the model simulation. Although the deposition was applied over the entire global ocean, we can neglect the impact of atmospheric deposition in other ocean basins on the North Atlantic Ocean due to the decadal time scales considered here. Seawater density is an indicator of the physical transport processes that affect the DINxs pool distribution. Modeled and observed upper ocean density distributions compared favorably (e.g. Fig. 5), suggesting that the model captured the important physical processes in the NASTG.

2.3 Biogeochemical model

Ecological interactions were simulated with a nutrient-phytoplankton-zooplankton-detritus (NPZD) type model similar to the one described in (Oschlies and Garçon, 1999). Modifications were made to increase the sinking speed of detritus linearly with depth (following a modified version of Eq. (6) in Kriest and Oschlies, 2008). After spinning up the physical model for 20 years, the ecosystem and circulation models were coupled online and run for 70 years with atmospheric deposition. The seven prognostic biogeochemical variables were dissolved oxygen, nitrate, phosphate, non-diazotrophic phytoplankton, zooplankton, and particulate detritus (one variable for detrital phosphorus and another for detrital nitrogen). Initial oceanic concentrations of nitrate, phosphate and oxygen were obtained from the World Ocean Atlas (WOA) 2001 (Conkright, 2002; Locarnini et al., 2002). Phytoplankton, zooplankton and detritus concentrations were obtained using a mmol N:mg chlorophyll ratio of 1.59 and setting initial detritus and zooplankton concentrations as 1% of the initial phytoplankton concentration. In the Redfield scenario, phytoplankton, zooplankton, and detritus are all simulated as the respective nitrogen equivalents, and phosphorus and oxygen fluxes are diagnosed from the nitrogen fluxes by applying the respective Redfield ratios. Export flux was determined from the product of detritus concentrations with the sinking velocity at approximately the base of the euphotic layer (100 m).

For comparison, a finer resolution model (1°×1° horizontal resolution and 50 vertical layers) was run for 42 years for the Redfield scenarios and compared to the coarser resolution runs. Within the NASTG region (20–32 N, 25–75 W), the one degree model NO_3^- and PO_4^{3-} nutriclines were similar in shape to the coarse model except that differences in surface physics depressed the nutrient gradients by about 50 m in the top 200 m (Fig. 6). This depression of the nutricline did not affect the magnitude of the nutrient deposition signal between 200–800 m for NO_3^-: at the end of the fine resolution model run, nutrient deposition caused an accumulation of 0.80 mmol NO_3^- m^{-3}, whereas in the fine resolution model there was an accumulation of 0.78 mmol NO_3^- m^{-3}

at year 42. Because the nutrient deposition accumulation signal includes both the relevant physical and biological dynamics, we determined that the coarse mode yielded similar results to the fine model, and so for computational reasons, the coarse resolution model was used for the sensitivity studies described in the remainder of the study.

As described earlier, two non-Redfieldian processes were simulated separately as mechanisms for excess N formation: preferential P remineralization of sinking particles and excess N uptake and export. In the preferential P remineralization scenario, detrital P was given a faster remineralization rate than detrital N in the euphotic layer (0.1 day^{-1} vs. 0.05 day^{-1}, respectively, Oschlies and Garçon, 1999). To ensure that DINxs profiles were realistic at depth, faster preferential remineralization of P occurred only in the euphotic zone (where the majority of labile organic P is thought to be regenerated Canellas, 2000). This condition required adding to the standard model a separate detrital phosphorus compartment.

In the excess N uptake scenario, our aim was to find the maximum amount of atmospheric DINxs that could be transported to the main thermocline from high N:P particles. For complete export to occur, we assumed two instantaneous processes: first, uptake of all atmospheric excess N by biogenic particles at the ocean surface (which would thereby increase their ratios to greater than Redfield); and second, the export and remineralization of these particles. Given these assumptions, we simulated the effect of atmospherically-derived high N:P particles on ocean biogeochemistry. Beginning at 100 m depth, where we assume that particles begin to remineralize upon export from the euphotic zone, we instantaneously distributed the deposited nutrients into the remineralization zone. The amount of mineralization at a given depth follows the average particulate organic matter remineralization profile in the model. Our assumptions allow no time delay for atmospheric nutrient export and ignore the impacts of lateral transport on the sinking particles. However, the focus of our study was on long-term changes and so the lack of time delay should not change the maximum effect deposition has on the DINxs pool if deposition increased N:P ratios in surface

BGD
6, 9849–9889, 2009

biogenic particles.

2.4 Isolation of the effects of nutrient deposition on ocean biogeochemistry

Denitrification, DOM formation and remineralization, and N_2 fixation were not included in the model due to our incomplete understanding of these non-Redfieldian processes in the gyre. Denitrification is not thought to be significant in the open North Atlantic water column (Hansell et al., 2007) and although data are scarce, continental shelf denitrification has not yet been demonstrated to have an effect on DINxs concentrations in the subtropical North Atlantic. Dissolved organic matter was excluded due to the paucity of data for DON and DOP concentrations in the subtropical gyre. Similarly to denitrification, excluding DOM was not a major problem because DOM does not sink, and any non-Redfield DOM formed from atmospheric nutrient deposition should exhibit a similar pattern as ADINxs in the Redfield (physical transport) scenario.

We could not realistically model N_2 fixation in the North Atlantic by simply assuming that diazotrophs have an advantage in surface waters with low excess N, i.e. a surplus of P over N (Deutsch et al., 2007; Schmittner et al., 2008). Its exclusion meant that we could not reproduce the observed DINxs pool nor maintain a realistic steady state of DINxs in the NASTG. Models such as that of Coles and Hood (2007) have dealt with the difficulty in maintaining realistic diazotroph levels by assuming that N_2 fixation equals the rate of development of the excess N signal. Since the goal here was to isolate the atmospheric contribution to the DINxs signal, this method was not an option.

We therefore did not include N_2 fixation in any of the model simulations and instead, we compared model runs with and without deposition, making the assumption that the various sources of DINxs are sufficiently independent to be superimposed linearly (see Fig. 7). This assumption enabled us to draw conclusions about the range of effects of atmospheric deposition in different scenarios without requiring that the model capture the entire complexity of the system. In order to isolate the effects that deposition has on excess N development, transient scenarios were run as replicates starting from World Ocean Atlas nutrient data. One replicate had atmospheric deposition while one

BGD
6, 9849–9889, 2009

did not. The difference between the replicates with and without deposition was taken as the isolated effect of deposition for that scenario. By comparing model runs with and without deposition, we were able to neglect N_2 fixation and other non-Redfieldian processes occurring and focus solely on the effects of excess N-deposition.

2.5 Production and loss rates of excess N

Model-simulated surface currents encircled the gyre approximately within the region defined by 20° N to 32° N and 25° W to 75° W (Fig. 8a). In this paper, the NASTG is taken to be the area within this region. The vertical zone of interest was defined as the depth range between 200 and 800 m. Although DINxs essentially moves along isopycnal (i.e., equal density) surfaces once it is formed, for several reasons we used depth surfaces instead of density surfaces as a vertical criterion. Firstly, the remineralization of sinking particles is one of the main vertical transport mechanisms of DINxs in our simulations. Sinking particles do not follow density lines but rather move through them vertically as they sink, making the degree of remineralization of these particles more related to depth than density. Secondly, the DINxs pool is bounded by different isopycnal surfaces in the western part of the gyre than in the eastern part because isopycnal surfaces deepen from east to west in the gyre while mineralization occurs at more uniform depths (Hansell et al., 2004). Finally, as the isopycnal layers deepen to the west, they mix with South Atlantic water, which masks the growth of DINxs there if density criteria are used (Hansell et al., 2004).

Within the NASTG region, a mass balance technique was used to approximate the production and loss rates of total DINxs. Assuming denitrification to be negligible, the only loss of DINxs is physical transport out of the NASTG. The model's circulation was applied to the observed DINxs field in the gyre in the absence of any DINxs inputs to estimate the loss from physical transport. The change in the observed DINxs pool was computed over a period of five years. Assuming that the North Atlantic is in steady state, we approximated the production rate of DINxs by equating it to the net loss rate of DINxs by transport out of the NASTG.

BGD
6, 9849–9889, 2009

Lastly, we compared the relative importance in each scenario of ADINxs input to total DINxs pool formation. About 55 years after nutrient deposition began, ADINxs accumulated at a constant rate between 200–800 m. We determined the mean annual growth of ADINxs in the subsequent 15 years, and this rate was taken to be the annual input rate of ADINxs into the gyre's main thermocline.

3 Results and discussion

3.1 Atmospheric nutrient deposition

Annually, there were 9.2 mmol N m^{-2} yr^{-1} and 0.064 mmol P m^{-2} yr^{-1} deposited to the NASTG, which, with an average ratio of 143:1, is much greater than the Redfield ratio. Our interest in modeling P deposition is to determine how deposited P affects the levels of excess N in deposition. Only the bioavailable fraction of deposited TP (which is predominantly SRP) will affect the surface nutrient balance. Here, in part because there are more TP deposition data than there are SRP deposition data, we attempted to obtain an overestimate of SRP deposition by modeling TP deposition and assuming all TP to be bioavailable. However, based on the literature measurements presented in Fig. 9 (which is based on the references in auxiliary material Table S2b in Mahowald et al., 2008), modeled TP deposition was an order of magnitude lower than observed TP data would suggest (about 19±35% of observed TP deposition). Modeled TP deposition (Fig. 4b) was closer in magnitude to observed SRP deposition; modeled wet TP deposition equaled 67±43% of observed SRP wet deposition (Table 1) (dry SRP deposition was not included due to scarcity of data). The differences between the modeled and observed TP fluxes indicate that our methods for estimating TP were inaccurate, although estimating SRP through TP was better.

Since SRP deposition is usually 2–3 orders of magnitude smaller than soluble inorganic N deposition (e.g. Markaki et al., 2003; Chen et al., 2007), our errors in SRP deposition estimation should have only minor effects on the amount of excess N in de-

BGD
6, 9849–9889, 2009

position. The southeast corner of the basin has the lowest modeled N:P ratio and it is only there that P fraction errors may be non-negligible. However, N:P ratios are still expected to be greater than Redfield (with deposition ratios of at least 37N:1P in the SE corner of the gyre and up to 310N:1P in the NW corner of the NASTG). The effects of atmospheric P on primary production itself is not the focus of this paper, but is assumed to have a relatively minor effect on marine ecosystem productivity on decadal time scales (Michaels et al., 1996).

3.2 Excess nitrogen production

3.2.1 Accumulation rates of DINxs in the NASTG

Based on loss rates of observed DINxs transported by the model's circulation out of the NASTG box (Sect. 2.5) and the assumption of steady state, annual DINxs productivity in the NASTG was estimated to be 2.7×10^{11} mol N yr^{-1}. This production rate can be compared with a previous independent estimate for the North Atlantic of $7.8\pm1.7\times10^{11}$ mol N yr^{-1} (Hansell et al., 2007). The Hansell et al. (2007) estimate was calculated from excess N spatial gradients and ventilation rates within the main thermocline of the North Atlantic. Because their estimate was calculated for the area over which the main thermocline is ventilated, it included sites that produce DINxs outside of the area defined in this study as the NASTG. This difference in areas may explain why our DINxs production rate was smaller than the Hansell et al. (2007) estimate. For the rest of this discussion, we use our modeled production rate.

Our estimate of the DINxs production rate has inherent errors. The initial DINxs concentrations were subject to analytical and interpolation errors within the initial WOA dataset. An error of 0.56 mmol m^{-3} was computed by taking the average of the standard deviations for each gridded point in the WOA dataset and including compounded analytical error in NO_3^- and PO_4^{3-} measurements. The error thus computed is likely to overestimate the error because it includes the variance both within and among sampling stations. Another uncertainty was in our assumption of steady state. The quantity

BGD
6, 9849–9889, 2009

of surface water that enters the main thermocline through springtime mode water subduction is highly variable interannually, affecting DINxs production and dilution in the main thermocline (Bates and Hansell, 2004). Therefore, the degree to which the WOA data represent a system in steady state depends on how well data from the individual cruises that made up the WOA dataset approach the DINxs climatic mean. However, this DINxs production rate can be used to approximate the importance of ADINxs (the atmospheric contribution to DINxs) to the total DINxs pool.

In the model scenarios, it took 55 years to reach a stable ADINxs accumulation rate between 200–800 m in the NASTG region. After this point, the Redfield, preferential P remineralization, and excess N uptake scenarios contributed, respectively, 18±0.5, 13±0.4, and 9±0.5 µmol ADINxs $m^{-3}\,yr^{-1}$ on average to sustain the DINxs pool with a direct atmospheric deposition of 5.4×10^{10} mol excess N yr^{-1} to the NASTG. Respectively, these contributions equal 27, 19 and 13% of the annual total DINxs production rate.

3.2.2 Spatial distributions of accumulation

The location of the ADINxs accumulation rate maximum between 200–800 m was spatially distinct from that of the majority of other DINxs sources. As discussed in Sect. 2.5, by assuming steady state, we defined DINxs production rates as equal, but opposite in sign, to the DINxs loss rates. By this definition, most DINxs was produced in the southern and western parts of the gyre (Fig. 10a). In contrast, most atmospheric N deposition originated in North America and was deposited into the northwestern NASTG (Fig. 4a).

As illustrated in Fig. 10b–d, mean ADINxs accumulated at different rates for each scenario but the location of the accumulation rate maximum was the same. The different rates were caused by the unique biological interactions with atmospheric nutrients at the surface in each scenario (described in detail in Sect. 3.3). While biological interactions were important to the overall rate of accumulation, the location of accumulation was mostly determined by the physical transport of water. When surface water nutrient

signatures formed from deposition at the surface (Fig. 11), they were then carried to the east by subtropical gyre currents, and were eventually subducted below 200 m in the northeastern part of the gyre. This pattern caused the accumulation of ADINxs to be fastest in the northeast.

When a density layer is used as a vertical criterion instead of a depth layer, similar maxima in ADINxs accumulation rates are observed in the northwest, although for different reasons (Fig. 12). ADINxs accumulates fastest at the surface (Fig. 11), and since isopycnals outcrop at the surface in the northeastern NASTG, the highest rates of ADINxs development were in the east. In contrast to the accumulation rates of ADINxs, the distribution of DINxs production rates within a density layer has a maximum to the west (Fig. 12a) because isopycnals deepening to the west intersect the depth layer that has the greatest production of DINxs.

3.3 Nutrient distributions and transport mechanisms

3.3.1 The Redfield scenario: ADINxs movement by physical transport

So far we have discussed accumulation rates of ADINxs in the three scenarios. Here, we describe the individual effects of each scenario and discuss their differences. We start with the Redfield scenario, in which all biological processes occurred in Redfield ratios so that the only mechanism for ADINxs to accumulate below the mixed layer from the surface is through physical transport of water and the tracers contained in it.

After 70 years in the Redfield scenario without N and P deposition, the absence of N_2 fixation in the model raised surface P to about 3 times higher levels than observed (up to 0.135 mmol m^{-3} P in 70 years from 0.049 mmol m^{-3} in the WOA data). In the Redfield scenario with deposition, the modeled addition of atmospheric nutrients briefly enhanced productivity and export from the surface, but the addition of excess N in the deposited nutrients caused surface P to essentially disappear (Fig. 11b). After P became fully depleted, continued deposition resulted in NO_3^- accumulation in the upper 100 m of the water column. During the 70 year model run, atmospheric nutrient de-

position caused surface NO_3^- in the NASTG to increase to levels much higher than currently observed (from WOA conditions of 0.16 to 0.31 mmol m^{-3}). Although their focus was the global ocean system rather than on the oligotrophic North Atlantic system, the modeling study of Krishnamurthy et al. (2007) also investigated the effects of nutrient deposition on surface biogeochemistry assuming Redfield conditions. Their results from 1990s level deposition likewise denote a global increase in surface N due to deposition (as indicated by a 1–2% increase in global primary productivity from the preindustrial era to the 1990s due to increased N and Fe solubility; Krishnamurthy et al., 2009.

Surface and subsurface circulation (Fig. 8) had a major affect on accumulation of ADINxs in the NASTG. Because most deposited N fell in the west (Fig. 4a), the Gulf Stream swept a sizeable fraction of it out of the NASTG region. However, in the Redfield scenario, ADINxs accumulated in the surface ocean instead of being exported. Therefore, when surface water re-entered the NASTG from the north and east (Fig. 8a), ADINxs from North America (and from Europe) was able to re-enter the gyre in surface and subducted water. Therefore, the Redfield scenario had the highest ADINxs accumulation (and retention of deposited material) in the NASTG between 200–800 m (Fig. 10b). In contrast, vertically exported ADINxs in the non-Redfield scenarios could not easily re-enter the gyre (note the net northward flow of 500 m water away from the northeast sector of the NASTG; Fig. 8b).

ADINxs subduction from surface waters alone cannot realistically explain empirical nutrient patterns in the NASTG, mainly because deposition raises modeled levels of surface N (Fig. 11b) to levels much higher than observed (Fig. 1; Wu et al., 2000; Li and Hansell, 2008). As a result, non-Redfield biological processes are likely to occur during or after assimilation of inorganic N from deposition. Nonetheless, describing the Redfield scenario is useful because it illustrates how nutrient distributions might change if excess N deposition were to become high enough to push the system further towards P limitation. In contrast to the observations, the Redfield scenario does not show the development of a subsurface DINxs maximum in the NASTG region (Fig. 10).

Also, although DOM was not specifically considered in this study, the Redfield scenario gives an indication of how subduction and remineralization of DOM will influence DINxs growth because semi-labile DOM should be similarly affected by physical transport as ADINxs in this Redfield scenario.

3.3.2 The preferential P remineralization scenario: a decoupling of N and P

We next consider how preferential P remineralization affected the distribution of deposited atmospheric nutrients in the ocean. The major difference from the Redfield remineralization scenario was that nutrient deposition did not cause complete P limitation in the surface. Biomass stimulated by deposition grew at Redfield ratios, but P remineralized faster than N when the biomass sank. The result was a spatial separation of remineralized N and P in the water column; of the nutrients taken up by organisms as a result of deposition, the preferential P remineralization run retained an additional 0.5 µmol P m^{-3} yr^{-1} in the NASTG surface compared to the Redfield run, and 13±0.4 µmol ADINxs m^{-3} yr^{-1} grew between 200–800 m (19% of the DINxs volumetric production rate; Sect. 3.2). The excess P in the surface layer allowed additional incoming ADINxs to be available to autotrophs. Thus, nutrient deposition resulted in greater overall nitrogen export from the surface compared to the Redfield scenario and it offered a mechanism by which ADINxs might be transported to depth.

As discussed in Sect. 2.4, these results are obtained by differencing two preferential P remineralization models: one with deposition and one without. By examining the difference between these two models, we are able to ignore biogeochemical interactions unrelated to deposition. However, in this case, the biogeochemical interactions unrelated to deposition offered interesting insights: we observed that in the models that included preferential P remineralization there were very strong biogeochemical perturbations from WOA conditions. Specifically, surface P increased (illustrated figuratively in Fig. 7) by 0.49 mmol P m^{-3} over 70 years in the NASTG, even though a decrease in surface P was observed when only the isolated effects of deposition were considered (illustrated as the downward arrow in Fig. 7). This meant that the overall effect

BGD
6, 9849–9889, 2009

of atmospheric excess N was not large enough to balance the excess P generated from production caused by non-deposition sources of nutrients. The signal was large enough that a much higher level of N deposition than modeled here would be necessary to counteract it. With the addition of preferential P remineralization, PO_4^{3-} in the main thermocline remained approximately the same on average as before, increasing a little in the area of the 18° water formation where surface water subducted into the gyre and decreasing in the areas surrounding the gyre. The increase in P at the surface was accompanied by severe N limitation and, as a result of P-rich surface water being subducted, a decrease in DINxs values in the main thermocline from 0.8 to $-3.5\,\mathrm{mmol\,m^{-3}}$ after 70 years.

A slower modeled preferential P mineralization rate may reduce differences from WOA conditions. However, the rate of preferential P remineralization used is probably a conservative estimate, based on the rapid turnover rate of phosphorus relative to nitrogen in surface waters (Benitez-Nelson, 2000). We conclude that if preferential P remineralization is to be responsible for the DINxs pool, it must occur in conjunction with one or more sources of excess N at the surface in addition to atmospheric deposition, such as N_2 fixation, in order to balance the excess P generated by preferential P remineralization at the surface.

For previously mentioned reasons, we did not include N_2 fixation in our model. Nonetheless, we can estimate the amount of N_2 fixation necessary in this scenario to sustain observed nutrient patterns in steady state: to balance the excess P at the surface, excess N from N_2 fixation should be equal to 16 times that of excess P. Or, in other words, if preferential P remineralization is the sole mechanism responsible for the high DINxs pool, excess N supplied at the surface from N_2 fixation should have the same magnitude as the amount of DINxs in the main thermocline.

For realistic nutrient distributions to occur in this scenario, the size of both the DINxs pool, and thereby the amount of N_2 fixation, is directly determined by the rate of preferential P remineralization. Basin-wide, the rate of preferential P remineralization in detritus is not known. We can estimate some upper and lower bounds for remineral-

BGD
6, 9849–9889, 2009

ization strength to be used in this scenario, by beginning with two assumptions: first, that preferential P remineralization is the only mechanism to contribute to the DINxs pool; second, that the DINxs pool is in steady state in the NASTG. Using an area of $8.13\times10^{12}\,m^2$ (for the NASTG as defined in this paper) and a DINxs production rate of $2.7\times10^{11}\,mol\,N\,yr^{-1}$ (from Sects. 2.5 and 3.2.1), we calculate that sinking particles must produce $0.033\,mol\,DINxs\,m^{-2}\,yr^{-1}$ to account for the observed DINxs pool within the NASTG. If all sinking particles were initially at Redfield ratios, the excess N at depth must be balanced by excess P at the surface. Based on our estimate of $0.033\,mol\,DINxs\,m^{-2}\,yr^{-1}$, therefore, 0.033/16, or $0.002\,mol\,excess\,P\,m^{-2}\,yr^{-1}$ should be generated in the surface. The strength of preferential P remineralization can then be calculated from the particle flux; the smaller the particle flux, the higher the preferential P remineralization rate must be in order to supply the excess P.

Unfortunately, export flux of PON from the surface of the NASTG to below the euphotic zone is not well constrained. Depending on the method used and the site and time sampled, N export flux in the NASTG ranges from <0.02 to $0.63\pm0.15\,mol\,N\,m^{-2}\,yr^{-1}$ (Jenkins, 1982, 1988; Jenkins and Goldman, 1985; Oschlies, 2002; Roussenov et al., 2006). If high and low-end estimates of export and DINxs annual production are used, anywhere between 5 and nearly 100% of original P in exported particles would need to remain in the surface. In fact, the low end estimates are too small to account for the DINxs itself. Given this wide range, we instead primarily focus on export flux and remineralization rates as relevant within our model.

We used a PON export flux of $0.08\,mol\,N\,m^{-2}\,yr^{-1}$, obtained from the first year of the Redfield model in order to approximate the climatological WOA conditions. Given a DINxs production rate of $2.7\times10^{11}\,mol\,N\,yr^{-1}$, we find that $0.003\,mol\,P\,m^{-2}\,yr^{-1}$ is removed from the surface, leaving $0.002\,mol\,P\,m^{-2}\,yr^{-1}$ at the surface as a result of preferential P remineralization. If the DINxs production rate is closer to the Hansell et al. (2007) estimate of $7.8\times10^{11}\,mol\,DINxs\,yr^{-1}$, then the total DINxs signal is larger than the export flux in our model. Having a DINxs signal larger than export flux in our model could indicate that either our export flux value is too small (e.g. because of the

BGD
6, 9849–9889, 2009

neglect of N_2 fixation) or that DINxs is laterally transported into the NASTG.

3.3.3 The excess N uptake scenario: ADINxs movement from high N:P biogenic particles

Finally, we investigated how nutrient distributions would change if biological nutrient uptake did not have to occur in Redfield ratios. In the case of atmospheric deposition, biomass should become N-enriched from the high N:P ratios available in nutrients from deposition. We obtained an upper estimate of ADINxs transport to below the euphotic layer by assuming in our idealized model that all atmospheric nutrients were immediately consumed upon deposition and then exported and remineralized in their original high N:P ratios.

As a result of the model stipulations, the excess N uptake scenario resulted in the most realistic distributions of nutrients. Nitrate and phosphate remained low in the surface and ADINxs developed between 200–800 m (Fig. 11d). Also, surface advection brought in less ADINxs from outside of the gyre since deposited nutrients were immediately removed from the surface waters by export. Therefore, the ADINxs accumulation rate between 200–800 m was smaller than in the other two scenarios (Fig. 10).

One unforeseen result was that we observed a decrease in surface P (Fig. 11d) at a rate of 0.6 $\mu mol\, m^{-3}\, yr^{-1}$; this result was surprising because surface nutrients were not directly altered by deposition. One possible cause for the surface P decrease is the upward mixing of ADINxs from within the subeuphotic zone with surface water, thus supporting surface production that results in the export of P. Consistent with this model observation, surface P in the North Pacific subtropical gyre is higher than in the NASTG (Moutin et al., 2008), perhaps in part because high DINxs water is not upwelled in this system (to the contrary, P-enriched waters underlie the surface Pacific). If export could be modeled in a more realistic way, this upwelled excess N should be immediately exported again once it became available at the surface. However, due to our model stipulations, we could not account for biological uptake in excess of Redfield ratios from upwelled water, and so this observation can probably not be interpreted as similar

BGD
6, 9849–9889, 2009

to what would happen in the real ocean. However, it is interesting that upwelling caused indirect changes in surface nutrients. This result indicates that upwelling may enhance the effect of deposition on the NASTG system because it resupplies ADINxs to the surface.

4 Conclusions

Atmospherically deposited nutrients of natural and anthropogenic origin have probably been affecting DINxs levels in the main thermocline of the NASTG for some time. By our estimates, atmospheric nutrient deposition could account for up to 19% of current annual DINxs production rates in the main thermocline. If N deposition continues to increase, deposition could greatly enhance the DINxs pool. The mechanisms and time scales by which atmospheric deposition will be transported out of the surface waters are unclear, although it appears that non-Redfield processes in the surface are important in the NASTG. Both preferential P remineralization and export of particles with a high N:P ratio could be the mechanisms responsible for transporting atmospheric DINxs out of the surface and into the main thermocline (although to produce realistic nutrient distributions, the preferential P remineralization requires N_2 fixation or higher levels of deposition to co-occur). In addition, all scenarios indicated that N deposition will increase P depletion in the NASTG.

Circulation of NASTG water was important to the fate of nutrient deposition in all three scenarios. Rapid ventilation of the gyre enabled atmospherically influenced surface water to be transported to the main thermocline, particularly affecting the northeastern part of the gyre in all scenarios. The rate of export was also important; the faster ADINxs was exported, the less accumulated in the NASTG. Because most atmospherically deposed nutrients landed near the Gulf Stream, a rapid export meant that when particles remineralized in deeper waters, they did not re-enter the gyre. In contrast, ADINxs transported in surface waters could re-enter. For this reason and due to the importance of surface water subduction in the NASTG, future studies would

BGD
6, 9849–9889, 2009

benefit by a more comprehensive inclusion of DOM. Finally, from the excess N uptake scenario it appears that convective upwelling may enhance the effects of deposition by resupplying atmospheric nutrients to the surface waters from below.

Our results indicate that atmospheric nutrient deposition is important enough to be included in future mass balance assessments of excess N in the NASTG. Based on our results, atmospheric N deposition will probably increase new production and affect surface as well as deep water concentrations of nutrients. Our results reinforce the idea that it is inappropriate to assume Redfield stoichiometry in this area.

Acknowledgements. We thank the AeroCom project (AeroCom Aerosol Comparisons between Observations and Models: http://nansen.ipsl.jussieu.fr/AEROCOM/, access: 2 September 2009), the Global Precipitation Climatology Project (Merged Satellite, Rain Gauge, and Model Precipitation Estimates: http://www.jisao.washington.edu/data/gpcp, access: 2 September 2009), and the IFM-GEOMAR biogeochemical modeling group and N. Mahowald, D. Olson, and J. Prospero for their helpful comments. L. Zamora and D. A. Hansell were supported by NSF Grant OCE-0623189.

References

Abell, J., Emerson, S., and Renaud, P.: Distributions of TOP, TON, and TOC in the North Pacific subtropical gyre: Implications for nutrient supply in the surface ocean and remineralization in the upper thermocline, J. Mar. Res., 58, 203–222, 2000. 9853

Aminot, A. and Kérouel, R.: Dissolved organic carbon, nitrogen and phosphorus in the N-E Atlantic and the N-W Mediterranean with particular reference to non-refractory fractions and degradation, Deep Sea Res. I, 51, 1975–1999, 2004. 9853

Antia, A.: Solubilization of particles in sediment traps: revising the stoichiometry of mixed layer transport, Biogeosciences, 2, 189–204, 2005, http://www.biogeosciences.net/2/189/2005/. 9853

Arrigo, K. R.: Marine microorganisms and global nutrient cycles, Nature, 438, 349–355, 2005. 9853

Bates, N. R. and Hansell, D. A.: Temporal variability of excess nitrate in the subtropical mode water of the North Atlantic Ocean, Mar. Chem., 84, 225–241, 2004. 9862

Benitez-Nelson, C. R.: The biogeochemical cycling of phosphorus in marine systems, Earth-Sci. Rev., 51, 109–135, 2000. 9866
Boyer, T. P., Stephens, C., Antonov, J. I., Conkright, M. E., Locarnini, R. A., O'Brian, T. D., and Garcia, H. E.: World Ocean Atlas 2001, Vol. 2: Salinity., 165 pp., 2002. 9855
Bronk, D. A.: Dynamics of DON, in: Biogeochemistry of Dissolved Organic Matter, edited by: Hansell, D. and Carlson, C., Academic Press, San Diego, 153–247, 2002. 9851
Canellas, M., Agusti, S., and Duarte, C. M.: Latitudinal variability in phosphate uptake in the Central Atlantic, Mar. Ecol.-Prog. Ser., 194, 283–294, 2000. 9857
Chen, L., Arimoto, R., and Duce, R. A.: The sources and forms of phosphorus in marine aerosol-particles and rain from northern New Zealand, Atmos. Environ., 19, 779–787, 1985. 9877
Chen, Y., Mills, S., Street, J., Golan, D., Post, A., Jacobson, M., and Paytan, A.: Estimates of atmospheric dry deposition and associated input of nutrients to Gulf of Aqaba seawater, J. Geophys. Res.-Atmos., 112, D04309, doi:10.1029/2006JD007858, 2007. 9851, 9855, 9860
Coles, V. J. and Hood, R. R.: Modeling the impact of iron and phosphorus limitations on nitrogen fixation in the Atlantic Ocean, Biogeosciences, 4, 455–479, 2007, http://www.biogeosciences.net/4/455/2007/. 9858
Conkright, M. E., Garcia, H. E., O'Brien, T. D., Locarnini, R. A., Boyer, T. P., Stephens, C., and Antonov, J. I.: World Ocean Atlas 2001, Vol. 4: Nutrients, in: NOAA Atlas NESDIS 52, Levitus, S., US Government Printing Office, Washington DC, 392, 2002. 9856
Dentener, F., Drevet, J., Lamarque, J. F., Bey, I., Eickhout, B., Fiore, A. M., Hauglustaine, D., Horowitz, L. W., Krol, M., Kulshrestha, U. C., Lawrence, M., Galy-Lacaux, C., Rast, S., Shindell, D., Stevenson, D., Van Noije, T., Atherton, C., Bell, N., Bergman, D., Butler, T., Cofala, J., Collins, B., Doherty, R., Ellingsen, K., Galloway, J., Gauss, M., Montanaro, V., Muller, J. F., Pitari, G., Rodriguez, J., Sanderson, M., Solmon, F., Strahan, S., Schultz, M., Sudo, K., Szopa, S., and Wild, O.: Nitrogen and sulfur deposition on regional and global scales: A multimodel evaluation, Global Biogeochem. Cy., 20, GB4003, doi:10.1029/2005GB002672, 2006. 9851, 9854
Deutsch, C., Sarmiento, J. L., Sigman, D. M., Gruber, N., and Dunne, J. P.: Spatial coupling of nitrogen inputs and losses in the ocean, Nature, 445, 163–167, 2007. 9852, 9858
Duarte, C. M., Dachs, J., Llabres, M., Alonso-Laita, P., Gasol, J. M., Tovar-Sanchez, A., Sanudo-Wilhemy, S., and Agusti, S.: Aerosol inputs enhance new production in the subtropical northeast Atlantic, J. Geophy. Res.-Biogeosci., 111, G040006,

doi:10.1029/2005JG000140, 2006. 9855
Duce, R. A., LaRoche, J., Altieri, K., Arrigo, K. R., Baker, A. R., Capone, D. G., Cornell, S., Dentener, F., Galloway, J., Ganeshram, R. S., Geider, R. J., Jickells, T., Kuypers, M. M., Langlois, R., Liss, P. S., Liu, S. M., Middelburg, J. J., Moore, C. M., Nickovic, S., Oschlies, A., Pedersen, T., Prospero, J., Schlitzer, R., Seitzinger, S., Sorensen, L. L., Uematsu, M., Ulloa, O., Voss, M., Ward, B., and Zamora, L.: Impacts of atmospheric anthropogenic nitrogen on the open ocean, Science, 320, 893–897, 2008. 9851, 9855
Fanning, K. A.: Nutrient provinces in the sea: Concentrations ratios, reaction rate ratios, and ideal covariation, J. Geophys. Res., 97, 5693–5712, 1992. 9851, 9852
Galloway, J. N., Howarth, R. W., Michaels, A. F., Nixon, S. W., Prospero, J. M., and Dentener, F. J.: Nitrogen and phosphorus budgets of the North Atlantic Ocean and its watershed, Biogeochem., 35, 3–25, 1996. 9851
Galloway, J. N., Townsend, A. R., Erisman, J. W., Bekunda, M., Cai, Z. C., Freney, J. R., Martinelli, L. A., Seitzinger, S. P., and Sutton, M. A.: Transformation of the nitrogen cycle: Recent trends, questions, and potential solutions, Science, 320, 889–892, 2008. 9851
Gnanadesikan, A., Dixon, K. W., Griffies, S. M., Balaji, V., Barreiro, M., Beesley, J. A., Cooke, W. F., Delworth, T. L., Gerdes, R., Harrison, M. J., Held, I. M., Hurlin, W. J., Lee, H. C., Liang, Z., Nong, G., Pacanowski, R. C., Rosati, A., Russell, J., Samuels, B. L., Song, Q., Spelman, M. J., Stouffer, R. J., Sweeney, C. O., Vecchi, G., Winton, M., Wittenberg, A. T., Zeng, F., Zhang, R., and Dunne, J. P.: GFDL's CM2 global coupled climate models. Part II: The baseline ocean simulation, J. Climate, 19, 675–697, 2006. 9855
Graham, W. F., Piotrowicz, S. R., and Duce, R. A.: The sea as a source of atmospheric phosphorus, Mar. Chem., 7, 325–342, 1979. 9855
Graham, W. F. and Duce, R. A.: The atmospheric transport of phosphorus to the western North-Atlantic, Atmos. Environ., 16, 1089–1097, 1982. 9877
Griffies, S. M., Gnanadesikan, A., Dixon, K. W., Dunne, J. P., Gerdes, R., Harrison, M. J., Rosati, A., Russell, J., Samuels, B. L., Spelman, M. J., Winton, M., and Zhang, R.: Formulation of an ocean model for global climate simulations, Ocean Sci., 1, 45–79, 2005, http://www.ocean-sci.net/1/45/2005/. 9855
Grimshaw, H. J. and Dolske, D. A.: Rainfall concentrations and wet atmospheric deposition of phosphorus and other constituents in Florida, USA, Water Air Soil Pollut., 137, 117–140, 2002. 9877
Gruber, N. and Sarmiento, J. L.: Global patterns of marine nitrogen fixation and denitrification,

Global Biogeochem. Cy., 11, 235–266, 1997. 9851, 9852
Hansell, D. A., Bates, N. R., and Olson, D. B.: Excess nitrate and nitrogen fixation in the North Atlantic Ocean, Mar. Chem., 84, 243–265, 2004. 9851, 9859
Hansell, D. A., Olson, D. B., Dentener, F., and Zamora, L. M.: Assessment of excess nitrate development in the subtropical North Atlantic, Mar. Chem., 106, 562–579, 2007. 9852, 9858, 9861, 9867
Herut, B., Krom, M. D., Pan, G., and Mortimer, R.: Atmospheric input of nitrogen and phosphorus to the Southeast Mediterranean: Sources, fluxes, and possible impact, Limnol. Oceanogr., 44, 1683–1692, 1999. 9877
Jenkins, W. J.: Oxygen utilization rates in North Atlantic subtropical gyre and primary production in oligotrophic systems, Nature, 300, 246–248, 1982. 9867
Jenkins, W. J.: Nitrate flux into the euphotic zone near Bermuda, Nature, 31, 521–523, 1988. 9867
Jenkins, W. J. and Goldman, J. C.: Seasonal oxygen cycling and primary production in the Sargasso Sea, J. Mar. Res., 43, 465–491, 1985. 9867
Karl, D. M. and Björkman, K.: Dynamics of DOP, in: Biogeochemistry of Dissolved Organic Matter, edited by: Hansell, D. and Carlson, C., Academic Press, San Diego, 249–366, 2002. 9852
Knapp, A. N., Hastings, M. G., Sigman, D. M., Lipschultz, F., and Galloway, J. N.: The flux and isotopic composition of reduced and total nitrogen in Bermuda rain, Mar. Chem., in press, 2009. 9852
Kriest, I. and Oschlies, A.: On the treatment of particulate organic matter sinking in large-scale models of marine biogeochemical cycles, Biogeosciences, 5, 55–72, 2008, http://www.biogeosciences.net/5/55/2008/. 9856
Krishnamurthy, A., Moore, J. K., Mahowald, N., Luo, C., Doney, S. C., Lindsay, K., and Zender, C. S.: Impacts of increasing anthropogenic soluble iron and nitrogen deposition on ocean biogeochemistry, Global Biogeochem. Cy., 23, GB3016, doi:10.1029/2008GB003440, 2009. 9864
Krishnamurthy, A., Moore, J. K., Zender, C. S., and Luo, C.: Effects of atmospheric inorganic nitrogen deposition on ocean biogeochemistry, J. Geophys. Res.-Biogeosci., 112, G02019, doi:10.1029/2006JG000334, 2007. 9851, 9864
Landolfi, A., Oschlies, A., and Sanders, R.: Organic nutrients and excess nitrogen in the North Atlantic subtropical gyre, Biogeosciences, 5, 1199–1213, 2008,

http://www.biogeosciences.net/5/1199/2008/. 9851, 9853
Large, W. G. and Yeager, S. G.: Diurnal to decadal global forcing for ocean and sea-ice models: The data sets and flux climatologies, Technical Report TN-460+STR, NCAR, 105 pp., 2004. 9855
Li, Q. P. and Hansell, D. A.: Nutrient distributions in baroclinic eddies of the oligotrophic North Atlantic and inferred impacts on biology, Deep-Sea Res. II, 55, 1291–1299, 2008. 9851, 9864
Locarnini, R. A., O'Brien, T. D., Garcia, H. E., Antonov, J. I., Boyer, T. P., Conkright, M. E., and Stephens, C.: World Ocean Atlas 2001, Vol. 3: Oxygen, in: NOAA Atlas NESDIS 51, Levitus, S., US Government Printing Office, Washington, DC, 286, 2002. 9856
Lomas, M. W., Swain, A., Shelton, R., and Ammerman, J. W.: Taxonomic variability of phosphorus stress in Sargasso Sea phytoplankton, Limnol. Oceanogr., 49, 2303–2310, 2004. 9853
Mahowald, N. M., Artaxo, P., Baker, A. R., Jickells, T. D., Okin, G. S., Randerson, J. T., and Townsend, A. R.: Impacts of biomass burning emissions and land use change on Amazonian atmospheric phosphorus cycling and deposition, Global Biogeochem. Cy., 19, GB4030, doi:10.1029/2005GB002541, 2005. 9854
Mahowald, N. M., Jickells, T. D., Baker, A. R., Artaxo, P., Benitez-Nelson, C. R., Bergametti, G., Bond, T. C., Chen, Y., Cohen, D. D., Herut, B., Kubilay, N., Losno, R., Luo, C., Maenhaut, W., McGee, K. A., Okin, G. S., Siefert, R. L., and Tsukuda, S.: Global distribution of atmospheric phosphorus sources, concentrations and deposition rates, and anthropogenic impacts, Global Biogeochem. Cy., 22, GB4026, doi:10.1029/2008GB003240, 2008. 9854, 9860
Markaki, Z., Oikonomou, K., Kocak, M., Kouvarkis, G., Chaniotaki, A., Kubilay, N., and Mihalopoulos, N.: Atmospheric deposition of inorganic phosphorus in the Levantine Basin, eastern Mediterranean: Spatial and temporal variability and its role in seawater productivity, Limnol. Oceanogr., 48, 1557–1568, 2003. 9851, 9860, 9877
Michaels, A. F., Olson, D., Sarmiento, J. L., Ammerman, J. W., Fanning, K., Jahnke, R., Knap, A. H., Lipschultz, F., and Prospero, J. M.: Inputs, losses and transformations of nitrogen and phosphorus in the pelagic North Atlantic, in: Nitrogen Cycling in the North Atlantic Ocean and its Watersheds, edited by: Howarth, R. W., Kluwer Academic Publishers, Dordrecht, Boston, 181–226, 1996. 9861
Moutin, T., Karl, D. M., Duhamel, S., Rimmelin, P., Raimbault, P., Van Mooy, B. A. S., and

Claustre, H.: Phosphate availability and the ultimate control of new nitrogen input by nitrogen fixation in the tropical Pacific Ocean, Biogeosciences, 5, 95–109, 2008, http://www.biogeosciences.net/5/95/2008/. 9868

Oschlies, A.: Can eddies make ocean deserts bloom? Global Biogeochem. Cy., 16, 1106, doi:10.1029/2001GB001830, 2002. 9867

Oschlies, A. and Garçon, V.: An eddy-permitting coupled physical-biological model of the North Atlantic – 1. Sensitivity to advection numerics and mixed layer physics, Global Biogeochem. Cy., 13, 135–160, 1999. 9856, 9857

Özsoy, T.: Atmospheric wet deposition of soluble macro-nutrients in the Cilician Basin, north-eastern Mediterranean sea, J. Environ. Monit., 5, 971–976, 2003. 9877

Pahlow, M. and Oschlies, A.: Chain model of phytoplankton P, N and light colimitation, Mar. Ecol.-Prog. Ser., 376, 69–83, 2009. 9853

Pahlow, M. and Riebesell, U.: Temporal trends in deep ocean Redfield ratios, Science, 287, 831–833, 2000. 9852

Peierls, B. L. and Paerl, H. W.: Bioavailability of atmospheric organic nitrogen deposition to coastal phytoplankton, Limnol. Oceanogr., 42, 1819–1823, 1997. 9855

Redfield, A. C., Ketchum, B. H., and Richards, F. A.: The influence of organisms on the composition of seawater, in: The Sea, Ideas and Observations on Progress in the Study of the Seas, edited by: Hill, M. N., Interscience, New York, 26–77, 1963. 9851

Roussenov, V., Williams, R. G., Mahaffey, C., and Wolff, G. A.: Does the transport of dissolved organic nutrients affect export production in the Atlantic Ocean? Global Biogeochem. Cy., 20(14), GB3002, doi:10.1029/2005GB002510, 2006. 9867

Schmittner, A., Oschlies, A., Matthews, H. D., and Galbraith, E. D.: Future changes in climate, ocean circulation, ecosystems, and biogeochemical cycling simulated for a business-as-usual CO_2 emission scenario until year 4000 AD, Global Biogeochem. Cy., 22, GB1013, doi:10.1029/2007GB002953, 2008. 9858

Seitzinger, S. P. and Sanders, R. W.: Atmospheric inputs of dissolved organic nitrogen stimulate estuarine bacteria and phytoplankton, Limnol. Oceanogr., 44, 721–730, 1999. 9855

Stephens, C., Antonov, J. I., Boyer, T. P., Conkright, M. E., Locarnini, R. A., O'Brian, T. D., and Garcia, H. E.: World Ocean Atlas 2001, Vol. 1: Temperature, 2002. 9855

Talbot, R. W., Harriss, R. C., Browell, E. V., Gregory, G. L., Sebacher, D. I., and Beck, S. M.: Distribution and geochemistry of aerosols in the tropical North-Atlantic troposphere – relationship to Saharan dust, J. Geophys. Res.-Atmos., 91, 5173–5182, 1986. 9877

Taylor, S. R. and McLennan, S. M.: The geochemical evolution of the continental crust, Rev. Geophys., 33, 241–265,1995. 9854

Van Mooy, B. A. S., Fredricks, H. F., Pedler, B. E., Dyhrman, S. T., Karl, D. M., Koblizek, M., Lomas, M. W., Mincer, T. J., Moore, L. R., Moutin, T., Rappe, M. S., and Webb, E. A.: Phytoplankton in the ocean use non-phosphorus lipids in response to phosphorus scarcity, Nature, 69–72, doi:10.1038/nature07659, 2009. 9853

Vidal, M., Duarte, C. M., and Agusti, S.: Dissolved organic nitrogen and phosphorus pools and fluxes in the central Atlantic Ocean, Limnol. Oceanogr., 44, 106–115, 1999. 9853

Williams, M. R., Fisher, T. R., and Melack, J. M.: Chemical composition and deposition of rain in the central Amazon, Brazil, Atmos. Environ., 31, 207–217, 1997. 9877

Wu, J., Sunda, W., Boyle, E. A., and Karl, D. M.: Phosphate depletion in the western North Atlantic Ocean, Science, 289, 759–762, 2000. 9851, 9864

Zamora, L., Hansell, D., and Prospero, J.: The organic nitrogen fraction of deposition over the North Atlantic, Geochim. Cosmochim. Acta, 73 (13, Supplement 1), A1498, 2009. 9855

Zhang, G. S., Zhang, J., and Liu, S. M.: Characterization of nutrients in the atmospheric wet and dry deposition observed at the two monitoring sites over Yellow Sea and East China Sea, J. Atmos. Chem., 57, 41–57, 2007. 9877

Table 1. Comparison of observed deposition fluxes of TP and SRP in wet deposition with our modeled TP deposition flux (mg m^{-2} yr^{-1}).

Lat. (N)	Long. (E)	Average annual wet deposition (cm)[a]	*n*	Observed wet SRP deposition	Modeled wet TP deposition	Reference
36.6	34.3	59	61	8.20	4.83	Özsoy (2003)
36.0	121.0	70	198	23.56	4.75	Zhang et al. (2007)
30.8	123.0	140	75	2.78	4.30	Zhang et al. (2007)
35.3	25.4	55	41	2.21	3.33	Markaki et al. (2003)
32.8	35.1	36	179	9.15	3.45	Herut et al. (1999)
31.8	34.7	18	57	9.15	3.45	Herut et al. (1999)
32.3	295.3	133	14	3.16	1.02	Graham and Duce (1982)
30.6	275.0	146	<149	1.26	0.99	Grimshaw and Dolske (2002)
30.0	277.8	129	<149	1.89	1.39	Grimshaw and Dolske (2002)
26.5	278.0	133	<149	1.89	1.33	Grimshaw and Dolske (2002)
25.3	279.3	133	<149	2.21	1.07	Grimshaw and Dolske (2002)
28.5	279.4	129	<149	1.58	1.10	Grimshaw and Dolske (2002)
13.2	300.5	77	2	6.94	5.26	Talbot et al. (1986)
−3.3	299.7	240	210	2.84	2.66	Williams et al. (1997)
−35	173	104	7	21.87	0.32	Chen et al. (1985)

[a] Deposition flux is inferred from the average annual rainfall obtained from the precipitation climatology of the Global Precipitation Climatology Project (GPCP) (http://www.jisao.washington.edu/data/gpcp).

BGD
6, 9849–9889, 2009

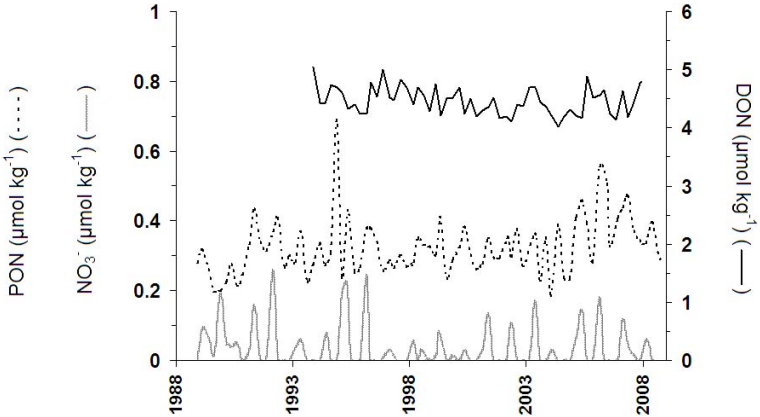

Fig. 1. Four-month seasonally averaged surface concentrations of nitrate (NO_3^-), particulate organic nitrogen (PON) and dissolved organic nitrogen (DON) at the Bermuda Atlantic Time-series Study station from 1988 through 2008. No noticeable increase in dissolved or particulate N is observed.

BGD
6, 9849–9889, 2009

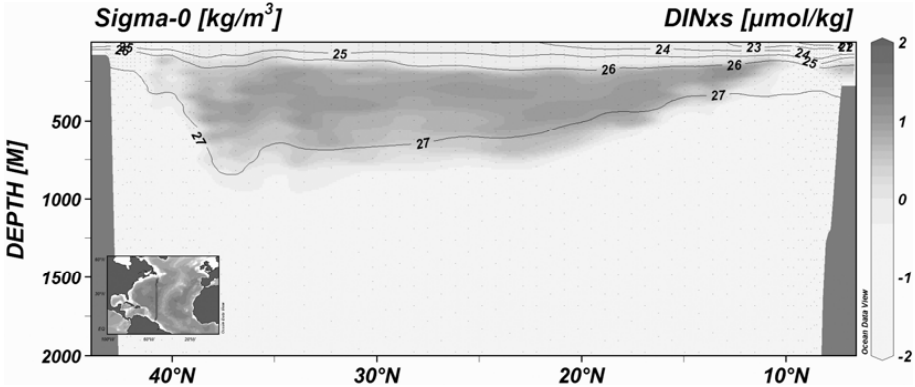

Fig. 2. Distribution of DINxs (gray scale) and sigma theta (line) from the 2003 CLIVAR A20 section. A high DINxs pool is observed between 26 and 27σ_θ (approximately 200–800 m).

BGD
6, 9849–9889, 2009

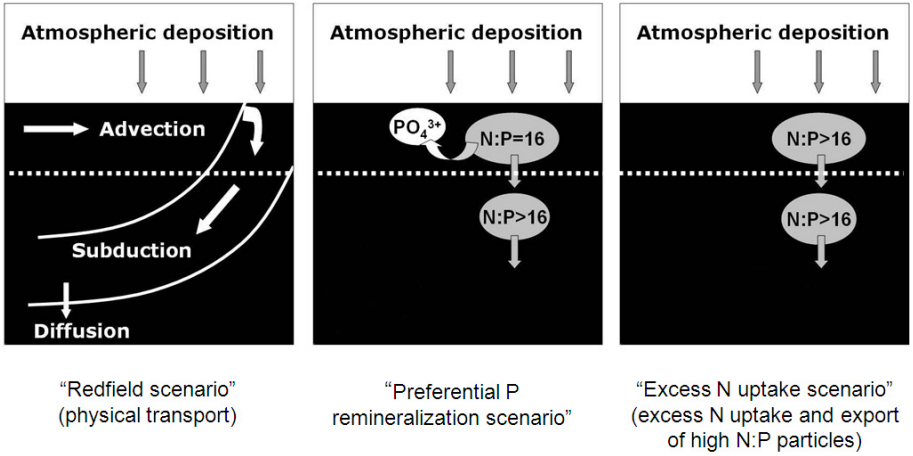

Fig. 3. Three mechanisms for the transport of atmospherically-deposited nutrients from the surface to below the ocean surface mixed layer. Nutrient deposition enhances biomass growth in all three scenarios. When biomass has Redfield N:P ratios (Redfield scenario), only vertical mixing can move from the surface to the main thermocline the high N:P material deposited from the atmosphere that remains after biological uptake. In the preferential P remineralization scenario, biomass loses phosphate preferentially as it sinks so that the remineralization of high N:P sinking particles at depth contributes to the DINxs pool. In the excess N uptake scenario, particles are produced and exported at high N:P ratios. Any of these scenarios could contribute to the transport of atmospheric nutrients from the surface to the main thermocline.

BGD
6, 9849–9889, 2009

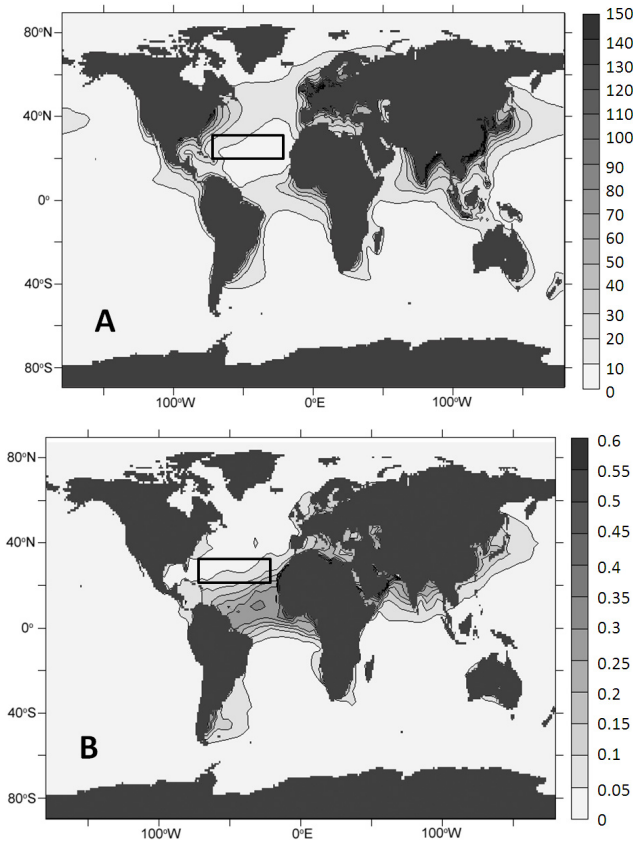

Fig. 4. Modeled atmospheric deposition to the North Atlantic. **(A)** Inorganic N deposition (mmol N m^{-2} yr^{-1}) **(B)** Total P deposition (mmol TP m^{-2} yr^{-1}). The NASTG region is outlined.

BGD
6, 9849–9889, 2009

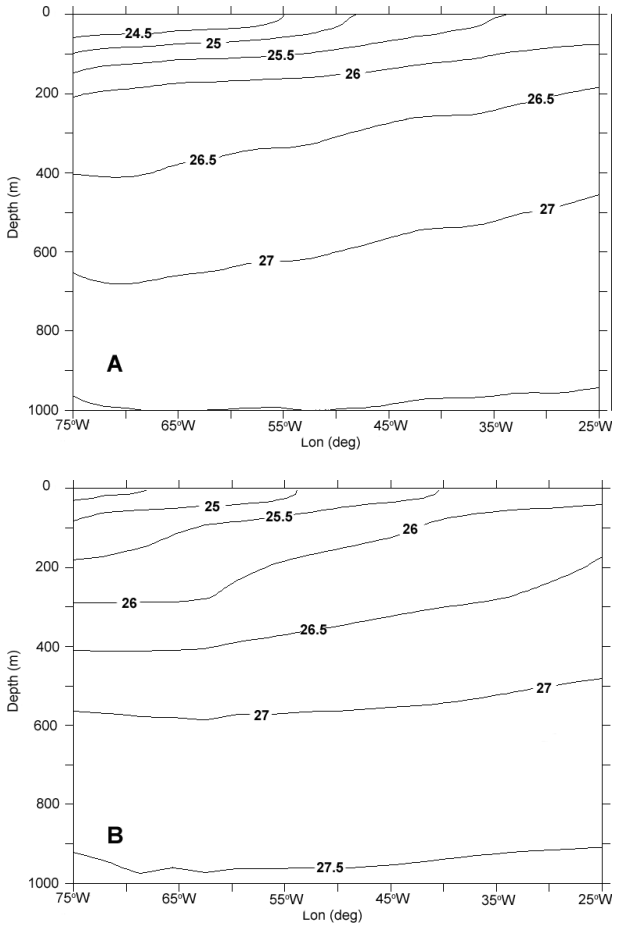

Fig. 5. Zonal cross-sections of density at 24.5° N **(A)** for World Ocean Atlas (WOA) and **(B)** for modeled data after 70 years of simulations.

BGD

6, 9849–9889, 2009

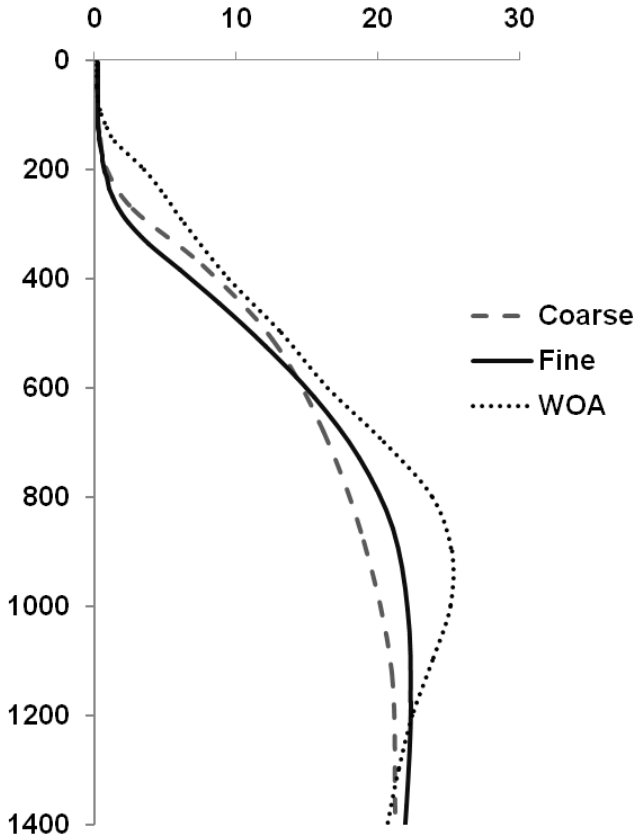

Fig. 6. Average nitrate concentrations (mmol m^{-3}) in the NASTG for WOA data and for the coarse and fine resolution Redfield models with deposition at year 42.

BGD
6, 9849–9889, 2009

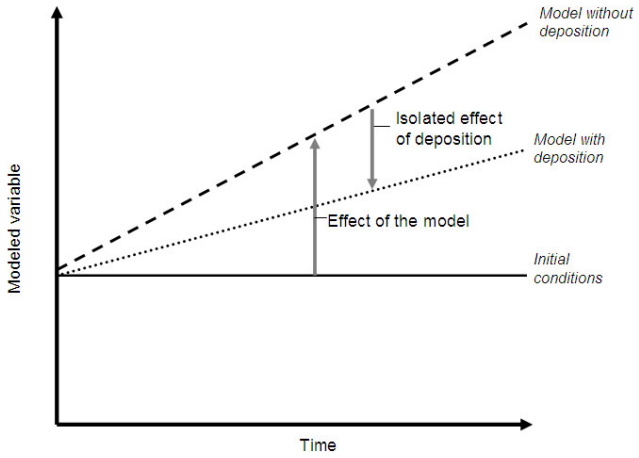

Fig. 7. An illustration of how the effect of deposition on a modeled variable (e.g. phosphate, nitrate, detritus, etc.) is determined. Over time, in this hypothetical case, the modeled variable strays from the initial conditions (for example, because of an inability to accurately model N_2 fixation and DOM). Assuming that atmospheric deposition affects the modeled variable independently of the absence of N_2 fixation and DOM, then the effects of deposition on the system can be isolated despite these deviations from initial conditions. After subtracting the model run without deposition from the run with deposition, we observe, in this hypothetical case, that deposition causes a net decrease in the modeled variable over time.

BGD
6, 9849–9889, 2009

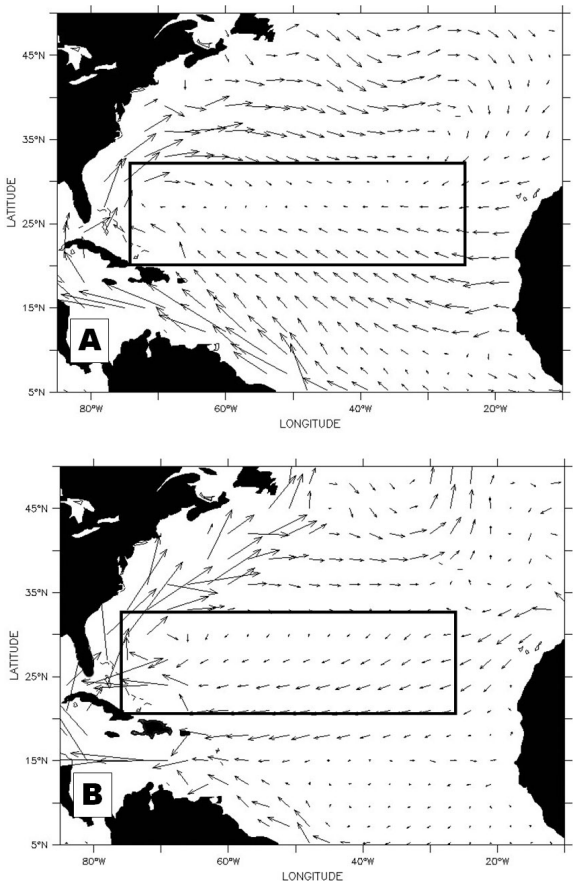

Fig. 8. Modeled year 70 circulation of the NASTG at **(A)** 5 m depth and **(B)** 500 m depth. The NASTG region is outlined.

BGD

6, 9849–9889, 2009

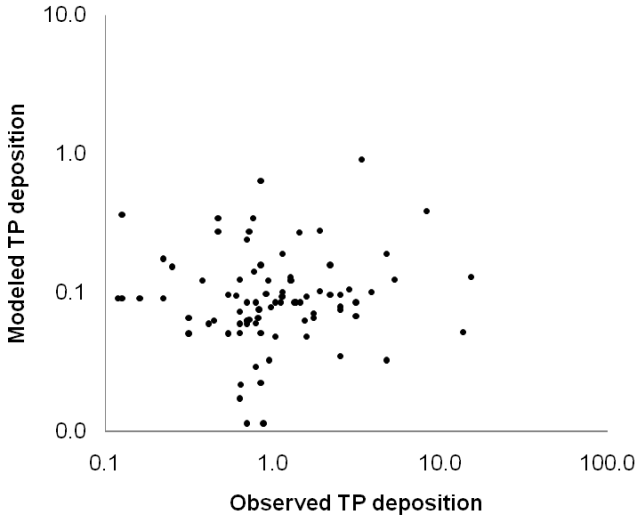

Fig. 9. A scatter plot comparing worldwide total P deposition observations and model estimates ($mg\,m^{-2}\,yr^{-1}$).

BGD
6, 9849–9889, 2009

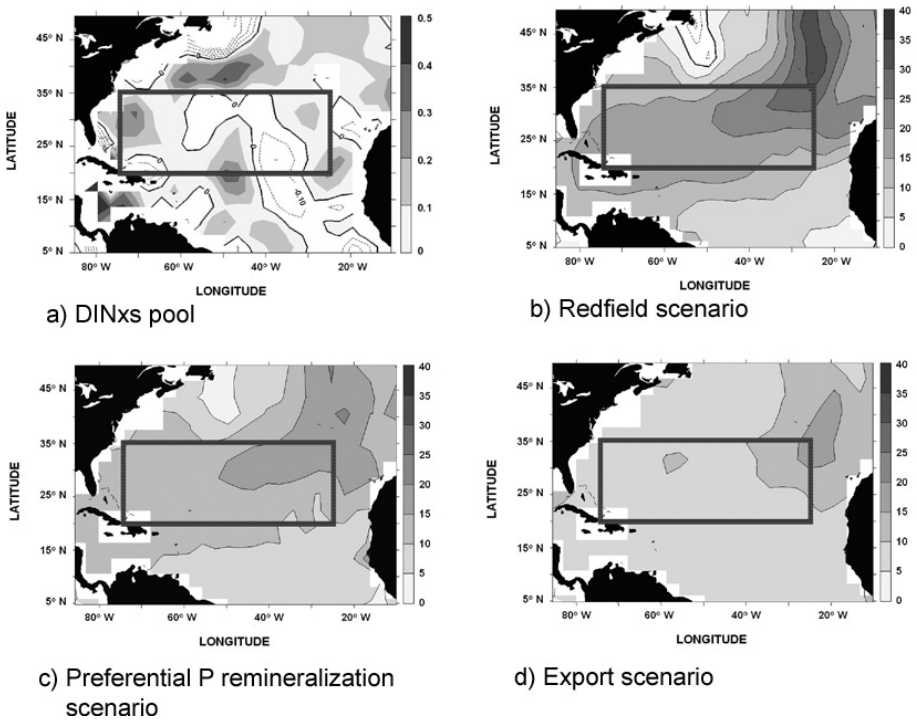

Fig. 10. Average accumulation rates between 200–800 m of **(a)** the total DINxs pool (mmol m^{-3} y^{-1}), and **(b–d)** the atmospheric contributions to the DINxs pool (ADINxs) in the three different scenarios (µmol m^{-3} y^{-1}). The NASTG region is outlined.

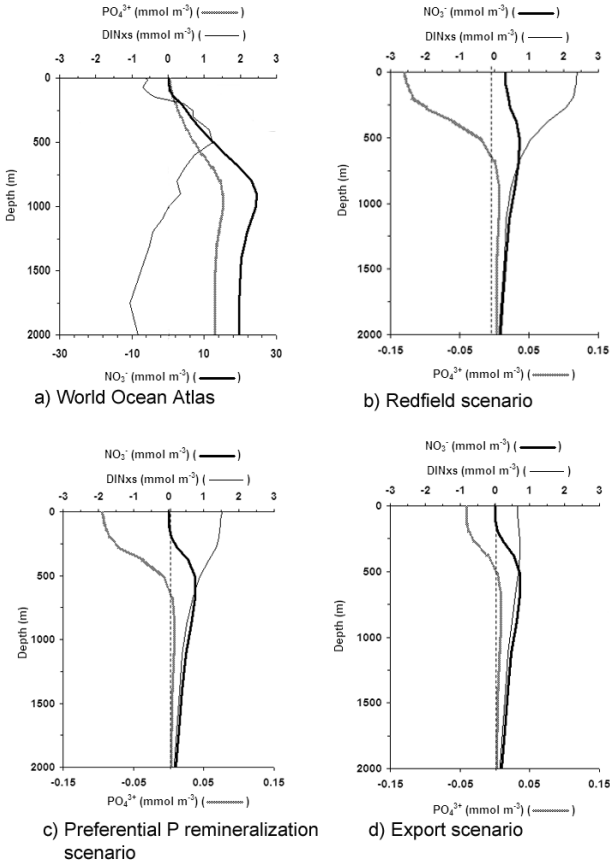

Fig. 11. Average NASTG nitrate, phosphate, and DINxs profiles of **(a)** World Ocean Atlas climatological observations (absolute values), and **(b–d)** the isolated effects of deposition for each scenario at model year 70 (deviation values). Deviations from the dashed line represent differences from the model run with no deposition.

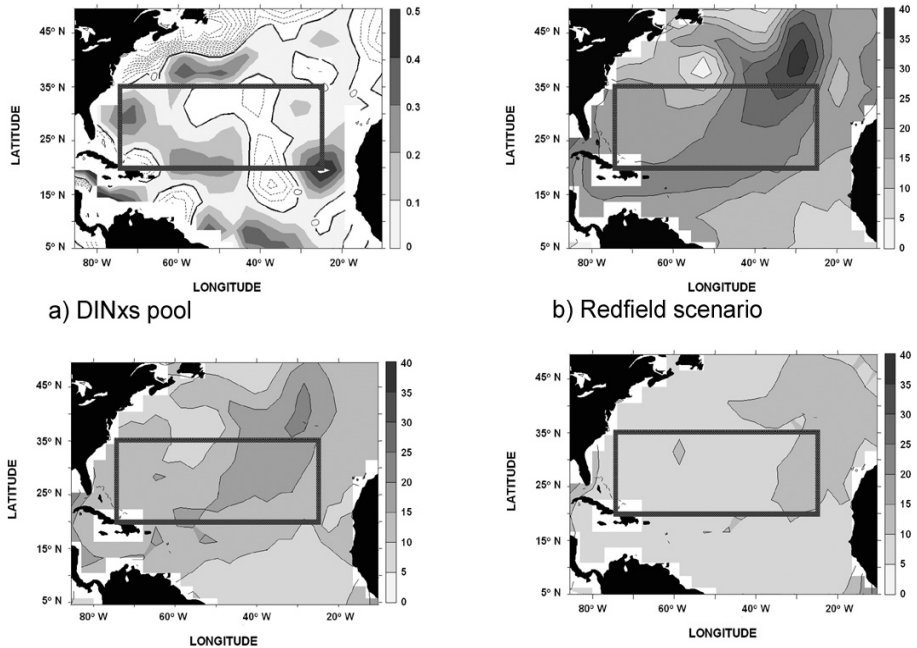

Fig. 12. Average accumulation rates between potential density surfaces σ_θ 26–27 of **(a)** the total DINxs pool (mmol m^{-3} y^{-1}), and **(b–d)** the atmospheric contributions to the DINxs pool (ADINxs) in the three different scenarios (μmol m^{-3} y^{-1}). The NASTG region is outlined.

BGD
6, 9849–9889, 2009